Laser-Ablation Profiles in Graphite: Application of the Heat-Balance Integral Method

Claude A. Klein* and Richard L. Gentilman*
Raytheon Company, Lexington, Massachusetts

The purpose of this work is to illustrate an application of the heat-balance integral method to the problem of describing and interpreting observations relating to crater formation in laser-irradiated polycrystalline graphite. Relevant experiments were carried out in the framework of a broadly based effort using a 12-kW continuous-wave DF laser facility; test runs of interest concern a fine-grained, nearly isotropic graphite grade known as GraphNOL. The paper focuses on two-dimensional ablation profiles generated in the course of both partial penetrations and complete burnthroughs of 3-mm-thick targets. Experiments performed on "flood-loaded" targets are examined in terms of the ablation history (crater depth, recession rate, backface temperature) and, subsequently, from the standpoint of time-integrated crater profiles. In this connection, it is demonstrated that accurate modeling of laser-induced craters must take account of the observation that off-axis irradiances fall off as the beam penetrates deeper into the target. Burnthrough tests performed on "large" specimens designed to assess the impact of enhanced lateral losses create additional problems. It is shown that the concept of an effective coupling coefficient can be extended to handle this case, thus confirming that the integral method provides a useful tool and adds to our understanding of continuous-wave laser-ablation dynamics in solids.

Nomenclature

C_p = target specific heat
$\mathcal{F}$ = nondimensional effective irradiance
H_A = thermochemical heat of ablation
H_V = heat of vaporization/sublimation
I = laser-beam intensity
K = target thermal conductivity
l = initial target thickness
P = laser-beam power
$\mathcal{P}$ = radiative power density
Q^* = effective heat of ablation
r = radial distance from centerline
t = elapsed time
T_V = target vaporization temperature
v_{SS} = steady-state recession rate
w = beam spot size ($1/e$)
α = target spectral emissivity
α_{eff} = effective coupling coefficient
ϵ_B = total emissivity, backface
ϵ_F = total emissivity, frontface
ζ = nondimensional axial variable
ζ_s = nondimensional surface position
η = target enthalpy parameter
θ = ablation surface angle
Θ = nondimensional temperature
κ = target thermal diffusivity
λ = thermal diffusion length
ρ = target mass density
σ_{SB} = Stefan-Boltzmann constant
τ = nondimensional elapsed time
τ_X = nondimensional exposure time

Presented as Paper 85-0940 at the AIAA 20th Thermophysics Conference, Williamsburg, VA, June 19-21, 1985; received July 8, 1985; revision received Aug. 15, 1986.

*Principal Research Scientist, Advanced Materials Department, Research Division.

I. Introduction

LASER-induced heating and laser-driven ablation of opaque solids both have been modeled successfully on the basis of the Fourier heat-conduction equation in conjunction with appropriate boundary conditions.[1] Exact solutions rely on the use of numerical techniques, which requires access to elaborate finite-difference codes and may not always be appropriate, considering the often large uncertainties in the thermophysical and thermochemical properties of contemplated "targets." Analytical procedures offer the advantage of providing simpler, though approximate, descriptions of laser-matter interactions and can be used to good advantage for interpreting experimental data or predicting the performance of laser-irradiated solids.[2] In this context, it is known that the heat-balance integral (HBI) method of Goodman[3] can be very attractive for expressing analytical solutions of laser-heating problems in closed form[4] or for reducing Stefan-type laser-ablation problems to ordinary initial-value differential equations.[5] The method makes rather drastic assumptions, especially with regard to the temperature dependence of key parameters such as the thermal conductivity and thermal diffusivity of the target. Still, even in those cases where temperature-dependent features play an important role, HBI-based procedures remain useful in describing how the ablation proceeds, that is, how the deposited laser energy drives the thermal front in competition with mass removal that occurs at the moving boundary. Furthermore, heat losses caused by convective transfer, surface reradiation, and lateral transport can be incorporated into the phenomenology by means of an "effective coupling coefficient"

$$\alpha_{eff} = \alpha - I_L/I \tag{1}$$

where α is the target absorptivity at the laser wavelength and I_L/I the fraction of incident irradiance that contributes to thermal losses.[5] In other words, α_{eff} measures the fraction of beam energy actually dissipated in the ablation process per se; for simple sublimators this includes bulk heating and surface vaporization. In this manner, we have demonstrated that the inherently one-dimensional HBI method can be extended to pseudo-two-dimensional situations, and that ablation features such as crater profiles created by Gaussian

beams can be modeled in accord with the results of code-based simulations performed elsewhere.[6]

The purpose of the present paper is to illustrate an application of the heat-balance integral method to the problem of describing and interpreting observations relating to crater formation in laser-irradiated polycrystalline graphite. Relevant experiments were carried out in the framework of a broadly based research effort[7] and made use of the United Technologies Research Center (UTRC) continuous-wave (cw) DF laser facility located at East Hartford, CT. Test runs of interest here concern a fine-grained, nearly isotropic graphite grade known as GraphNOL,[8] which was originally developed for special service in the aerospace and nuclear industries. This high-quality product can withstand extreme conditions of thermal shock as encountered in a re-entry environment and, consequently, promises to provide an ideal candidate material for evaluating "true" thermochemical ablation occurring in a graphitic sublimator subjected to rapid heating rates. The paper focuses on two-dimensional ablation profiles generated in the course of both partial penetrations and complete burnthroughs of 3-mm-thick GraphNOL targets. These profiles are assessed in the light of HBI-based calculations taking into account the spatial distribution of the incident radiation; in effect, the integral method turns out to be quite satisfactory, thus confirming our basic understanding of cw laser-ablation dynamics in graphite.

The paper is structured as follows. First, the experimental procedure is presented (Sec. II), that is, specifics on beam intensity and beam shape are provided in addition to a description of the techniques used for measuring burnthrough times and obtaining ablation contours. Concepts and equations of relevance in applying the HBI method to the problem on hand are summarized in Sec. III, for the benefit of the reader who may not be familiar with the content of Ref. 5. In this context, it will be shown that test runs of interest here reflect "low-intensity" situations in the sense that they involve a direct transition from preablation (Phase I-B) to ablation in a Phase-III-type mode, thus pointing to nonsteady-state dynamics throughout the burn. Experiments performed on "flood-loaded" 15-mm-diam targets are examined in Sec. IV, not only from the standpoint of "time-integrated" crater profiles but also in terms of the ablation history as portrayed by on-axis crater depth, recession rate, and backface temperature. In this connection, it will be demonstrated that accurate modeling of laser-induced craters must take account of the observation that off-axis irradiances may fall off as the beam penetrates deeper into the target. Burnthrough tests performed on "large" specimens (30 mm in diameter) and designed to assess the impact of enhanced radial losses create additional problems. In Sec. V, it is shown how the concept of an effective coupling coefficient can be extended to handle this case, thus throwing new light on the nature of the interaction process. Primary implications of our work, particularly with regard to energy partitioning in laser-irradiated GraphNOL, are discussed in Sec. VI; implications in terms of spot-size scaling and effective heat of ablation will be considered in a forthcoming paper.[9]

Table 1 GraphNOL laser-irradiation test runs: key experimental data

Run no.	D, mm	l, mm	P,[a] kW	I_0, kW/cm^2	t_X, s	t_{BT}, s
74-91	15	3.06	5.42	7.4	5.84	5.55
74-92	15	3.17	5.42	7.4	4.44	N/A
74-93	15	3.17	5.49	7.5	2.22	N/A
74-96	15	2.92	12.95	18.6	1.49	1.42
74-97	15	2.97	12.95	18.6	1.13	N/A
75-48	30	3.07	12.54	18.0	1.645	1.57

[a]After truncation (1.60×1.60 cm).

II. Experimental Procedure

A detailed description of the UTRC laser facility, including procedures used for the test runs, is given in Ref. 7. Briefly, the UTRC laser operates at the DF (3.8 μm) wavelength and outputs a cw beam of up to 12-kW nominal power distributed over a square aperture of 1.6×1.6 cm. By varying the laser-output power, peak intensities of about 7–19 kW/cm^2 were obtained in the test chamber and were found to fluctuate by less than 10% over the duration of a typical test run. Constant-intensity contours were nearly circular, but radial distributions had multimode features in the sense that smoothed three-dimensional representations were found to be almost conical in the central region. Azimuthally averaged beam-intensity measurements are displayed in Fig. 1 and are seen to obey a fourth-order polynomial dependence:

$$I(r)/I_0 = 1.000891 - 0.7902083r - 2.808854r^2 + 4.130208r^3 - 1.516927r^4 \quad (2a)$$

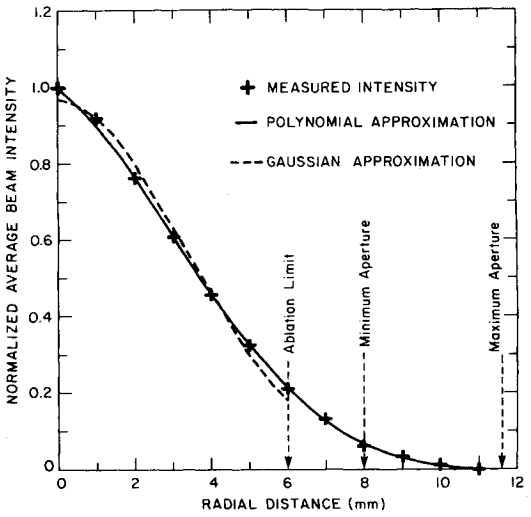

Fig. 1 Laser-beam shape: measured intensities, exact radial dependence, and Gaussian approximation.

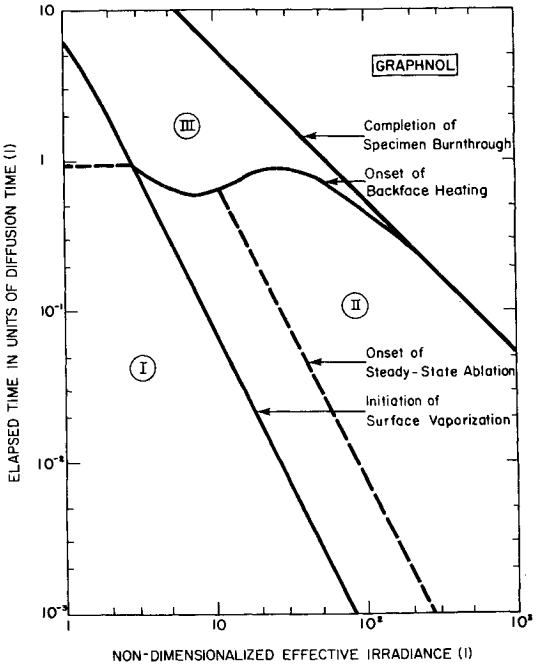

Fig. 2 Time/irradiance domains for phases I–III in laser-irradiated GraphNOL.

Note that, for the sake of convenience, and since ablation occurred at radial distances of no more than 6 mm, we have chosen to describe the beam-intensity distribution by means of a Gaussian function (see Fig. 1); for the purpose of the present investigation, we take it that the beam shape can be approximated by means of

$$I(r)/I_0 \simeq 0.965 \exp[-(r/0.462)^2] \tag{2b}$$

if r is the radial distance in centimeters, keeping in mind that Eq. (2b) was derived from a bivariate regression using Marquardt's algorithm.[10]

The six GraphNOL ablation experiments considered herein (see Table 1) were all conducted in an argon environment at a controlled pressure of 9 Torr. The target specimens were in the form of disks, about 3-mm thick, and measured 15 mm in diameter (standard diameter) except for test run 75-48; the surfaces were smooth, with no coating or treatment of any kind. On assuming that any laser-light absorption by ablation products was minimal,[7] the peak intensities listed in Table 1, which reflect the results of carefully calibrated beam-power measurements, should be indicative of time-averaged incident peak irradiances. As outlined in the Introduction, many of the present experiments were directed at obtaining accurate burnthrough times because this technique yields steady-state recession rates,[5]

$$v_{SS} = l/t_{BT} \tag{3}$$

thus providing effective heats of ablation without involving the problems that arise if one attempts to interpret the results of partial-penetration or mass-loss-type experiments. In this connection, we note that exposure to laser light was controlled by an electromechanical shutter, which took approximately 25 ms to fully operate, both ways; the shutter opening was activated by a mechanical switch, whereas shutter closing was triggered by an electrical signal from either an adjustable timer or a burnthrough detector. In the latter case, and due to variations in geometrical alignment and detector response, there were delays ranging from approximately 0.05 to 0.35 s before the shutter closed, which resulted in burnthrough holes 1-2 mm in diameter, at the bottom of the crater. The burnthrough times listed in Table 1 were obtained from videotape recordings: An event marker signaled the start of shutter opening, while the first visible evidence of a hole in the target was taken to signal burnthrough. At a 60-Hz frame rate, the total uncertainty affecting measured burnthrough times thus should not exceed 30 ms.

Ablation craters were profiled with the help of a Nikon optical microscope, after mounting the irradiated specimens onto standard glass slides. In view of the limited depth of field at 100× magnification, the relative distance from the lens to any point on the specimen's surface could be accurately determined (±0.01 mm) from the calibrated scale on the mechanical knob that adjusts the fine focus. The X-Y stage, which has two Vernier scales, is accurate to ±0.1 mm. Radial profiles were obtained by first locating the point of maximum depth of the crater, or the center of the hole in the case of burned-through targets, and recording its X-Y position; this position was defined as station $r=0$. Then, and along four orthogonal axes (north, south, east, west), the radial distance was recorded for a number of height increments ΔZ, with "north" assigned to the top of the target as irradiated. The ΔZ increments (0.2–0.5 mm) were selected depending on the depth of the crater.

Table 2 Pertinent physical properties of GraphNOL

Mass density, ρ	1.85g-cm^{-3}
Sublimation temperature,[a] T_V	3600 K
Heat of vaporization, H_V	26.5 kJ-g^{-1}
Specific heat,[b] $\overline{C_p}$	1.79 J-g^{-1}K^{-1}
Thermal conductivity,[b] $\overline{K}$	0.602 W-cm^{-1}K^{-1}
Spectral emissivity,[c] α	0.93±0.09

[a]Tentative value at 0.01 atm (Ref. 12). [b]Average value for 290 ≤ T ≤ 3600 K (Ref. 13). [c]At 3.8 μm for a vaporizing surface (Ref. 14).

III. Analytical Procedure

The critical step in applying the HBI method to realistic laser-ablation problems boils down to obtaining an appropriate effective coupling coefficient in the sense of Eq. (1). Since α_{eff} is the fraction of incident fluence actually dissipated in ablating the target, energy-conservation considerations require that

$$\alpha_{eff} = \rho l H_A/(t_{BT} I) \tag{4}$$

if I refers to the beam intensity that causes burnthrough, and the other symbols are as specified in the Nomenclature. The thermochemical heat of ablation

$$H_A = H_V + \int_{T_0}^{T_V} C_p(T)\,dT \tag{5}$$

includes the heat of vaporization at the sublimation temperature and the change in heat content per unit mass of target material as the temperature increases from T_0 to T_V. At this point, we may introduce the dimensionless enthalpy parameter η,

$$\eta = \frac{H_V}{\overline{C_p}(T_V - T_0)} \tag{6}$$

where $\overline{C_p}$ is the average specific heat for temperatures ranging from T_0 to T_V, and rewrite Eq. (5) as follows:

$$H_A = (1+\eta)\overline{C_p} T_V' \tag{7}$$

if temperatures T' are measured on a scale that sets T_0 equal to zero. For GraphNOL, with physical properties as given in Table 2, we have $\overline{C_p} T_V' = 5.9$ kJ/g and $\eta = 4.5$, which suggests that $H_A \simeq 32.5$ kJ/g should be a "good number" for the heat of ablation, in a vacuum environment. Note that the recommended heat of vaporization of about 26 kJ/g (see, for instance, Ref. 11) is well below the enthalpy required to sublime graphite to monoatomic carbon under equilibrium conditions (59 kJ/g) and reflects the well-documented observation that graphite sublimes to molecules such as C_3 and C_5, as well as to single atoms.

If the deposition of laser energy occurs in a surface layer of infinitesimal thickness, the temperature evolution[15] of a finite-thickness slab having an insulated backface can be formulated in a completely nondimensional manner on making use of dimensionless variables for the temperature increase ($\Theta = T'/T_V'$), the distance from the front surface ($\zeta = z/l$),

Table 3 GraphNOL laser-irradiation test runs: nondimensionalized key parameters

Run no.	α_{eff}	$\mathfrak{F}$[a]	$\Theta(1,\tau_V)$[a]	τ_V[a]	τ_X	I_L/I_0
74-91	0.447	0.508	0.746	16.2	112	0.483
74-92	0.447[b]	0.526	0.737	15.5	79.4	0.483
74-93	0.447[b]	0.533	0.734	15.2	39.7	0.483
74-96	0.663	1.81	0.165	2.37	31.4	0.267
74-97	0.663[b]	1.84	0.156	2.29	23.0	0.267
75-48	0.51 [c]	1.81	0.166	2.37	31.4	0.42[c]

[a]On centerline. [b]Postulated value (no burnthough). [c]Average value (see Sec. V).

and the elapsed time ($\tau = t/t_d$). The diffusion time t_d refers to axial transport and is given by

$$t_d = l^2/(\pi^2\kappa) \tag{8}$$

with a diffusivity set equal to $\bar{K}/(\rho\bar{C}_p)$, where $\bar{K}$ represents an average thermal conductivity defined in accord with the prescription for $\bar{C}_p$. Such a procedure (see Ref. 5) immediately suggests expression of the irradiance in units of $\bar{K}T'_V/l$, keeping in mind that this is precisely the irradiance that generates a temperature gradient equal to $-T'_V/l$ at the frontface. In units of this "nominal" irradiance, an effective irradiance amounts to

$$\mathcal{F} = \alpha_{\text{eff}} Il/(\bar{K}T'_V) \tag{9a}$$

or

$$\mathcal{F} = \rho l^2 H_A/(t_{\text{BT}}\bar{K}T'_V) \tag{9b}$$

and, thus, no longer explicitly depends on the beam intensity. For orientation purposes, we may insert experimental data and property values as listed in Tables 1 and 2, which leads to the conclusion that all of our experiments verify the condition $\mathcal{F} \leq 1.84$ (see Table 3). Now consider Fig. 2, which delineates the three "time-irradiance" domains that correspond to Phase I, II, and III-type phenomenologies in laser-irradiated GraphNOL: It is seen that, in our experiments, the entire ablation evolves in a Phase III mode.

In this light, we take it that the normalized front-surface position ζ_s ($\zeta_s = 0$ at the onset of ablation) is a solution of the following differential equation[5]:

$$\frac{d}{d\tau}\left[\zeta_s(\tau)\right] = \frac{3}{\pi^2\eta}\left[1 - \Theta(1,\tau_V) - \frac{1-\Theta(1,\tau)}{1-\zeta_s(\tau)}\right] \tag{10}$$

where $\Theta(1,\tau)$ represents the backface temperature. At the onset of ablation, this temperature is equal to $\Theta(1,\tau_V)$ and then evolves in accord with

$$1 - \Theta(1,\tau) = \frac{1-\Theta(1,\tau_V) + (e\eta/2)\zeta_s(\tau) - (e\mathcal{F}/2\pi^2)(\tau-\tau_V)}{1-\zeta_s(\tau)} \tag{11}$$

if e stands for exp(1). These two coupled equations control the entire evolution of the ablation ($\tau_V \leq \tau \leq \tau_X$) in the sense that the solution yields the penetration history, which leads to the backface temperature, which in turn provides the recession rate through insertion of $\zeta_s(\tau)$ and $\Theta(1,\tau)$ into Eq. (10). Initial conditions include the vaporization time and the backface temperature at vaporization; both are best obtained from a preablation model patterned upon the classic slab-heating equation of Ref. 15. In Ref. 5 it is shown that, for all practical purposes, we may write

$$\tau_V = \pi^2(1/\mathcal{F} - 1/3) \text{ if } \mathcal{F} \leq 1.6 \tag{12a}$$

and

$$\tau_V = 7.72/\mathcal{F}^2 \text{ if } \mathcal{F} > 1.6 \tag{12b}$$

By the same token, the backface temperature at vaporization is simply

$$\Theta(1,\tau_V) = 1 - \mathcal{F}/2 \tag{13a}$$

if $\mathcal{F} \leq 1.6$ and can be approximated by means of

$$\Theta(1,\tau_V) = 0.0384\mathcal{F}(7.72/\mathcal{F}^2 - 0.627)^{1.57} \tag{13b}$$

for $1.6 < \mathcal{F} \leq 3.0$, which confirms that, indeed, we always had a hot backface when ablation commenced (see Table 3).

IV. Small Targets

Since GraphNOL has a thermal diffusivity of about 0.2 cm^2/s, at high temperatures, it is easy to verify that, in our experiments, the diffusion length at burnthrough,

$$\lambda = \pi\sqrt{\kappa t_{\text{BT}}} \tag{14}$$

was of the order of 15 mm or more. Considering the $1/e$ spot-size radius of the incident beam ($w \simeq 4.6$ mm), it appears that radially directed heat flow played a significant role in the interaction process. Furthermore, for 15-mm-diam targets, we note that the diffusion length verifies the condition $\lambda > D/2$, which should be indicative of a thermal equilibrium situation; for reasons that will become clearer later on, such targets will be referred to as "small."

Take test run 74-96: On axis, and according to Eq. (9b), the nondimensionalized effective irradiance is equal to 1.81, which indicates that $\Theta(1,\tau_V)$ and τ_V are both as given in Table 3. Returning now to Eq. (10) and setting the enthalpy parameter equal to 4.5, it is seen that, on axis, the surface recession $\zeta_s(\tau)$ obeys a nonlinear differential equation best expressed as follows:

$$\frac{d\zeta_s(\tau)}{d\tau} = 0.0678\left[0.835 - \frac{1-\Theta(1,\tau)}{1-\zeta_s(\tau)}\right] \tag{15}$$

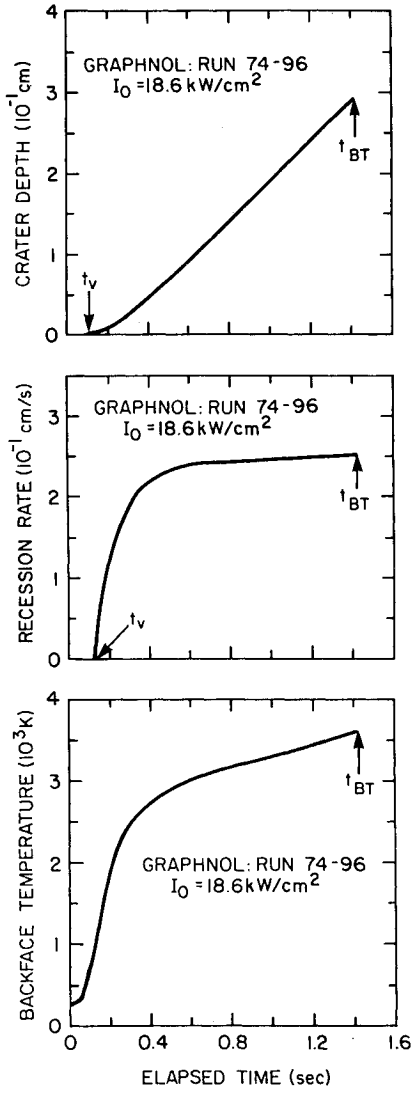

Fig. 3 Calculated, on-axis laser-ablation history: test run 74-96.

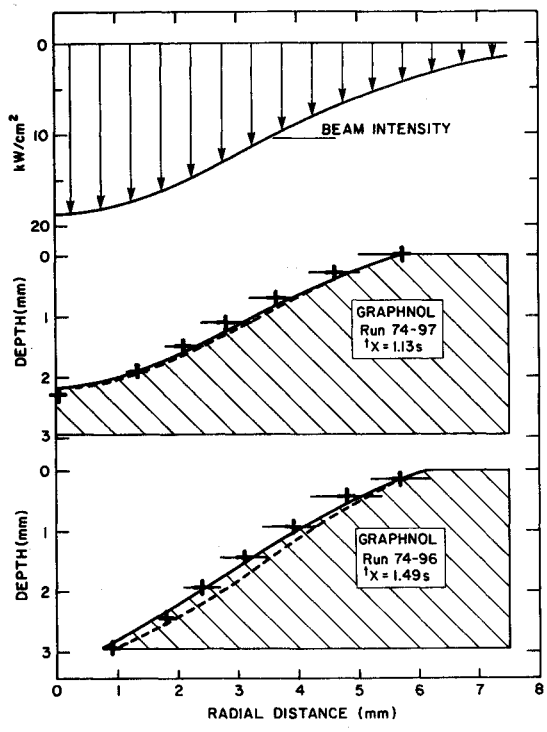

Fig. 4 Measured and calculated ablation profiles; the dashed lines illustrate analytical results that do not take the slope of the crater into consideration.

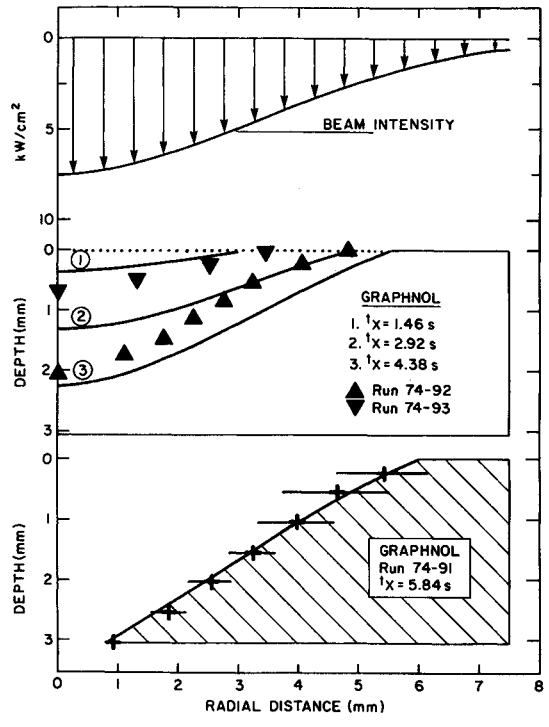

Fig. 5 Measured and calculated ablation profiles at peak intensities of 7.4 kW/cm².

where

$$1-\Theta(1,\tau)=\frac{0.835+6.09\zeta_s(\tau)-0.249(\tau-2.37)}{1-\zeta_s(\tau)} \tag{16}$$

specifies the evolution of the backface temperature and $\zeta_s(2.37)=0$ provides the initial value. The solution of this system, for $\tau=\tau_V$ to $\tau=\tau_{BT}$, can be obtained by means of a fourth-order Runge-Kutta procedure with a step size that must be chosen with some care because of potential "instabilities" that may develop when the receding front surface approaches the backface. For test run 74-96, and after converting to properly dimensionalized variables, the solution yields crater-depth, recession-rate, and backface-temperature histories as displayed in Fig. 3. Observe how the "transient" phase, immediately after the onset of surface vaporization, is giving rise to a relatively long period of quasistationary ablation, the surface receding at an almost constant velocity. In this connection, it is recalled that the HBI method yields[5]

$$v_{BT}=v_{SS}(1+\eta)/\eta \tag{17}$$

for the terminal burn velocity, which means 0.252 cm/s in our case, with v_{SS} as in Eq. (3); this is in excellent agreement with the result of the numerical integration (see Fig. 3), thus confirming that the present procedure is indeed consistent and reliable.

For the purpose of modeling the ablation contour of full and partial burns as recorded in Fig. 4, we may "image" the transverse variation in beam intensity simply by substituting $I_0\exp(-r^2/w^2)$ for I in Eq. (9a). Since $\mathcal{F}_0$ should be almost identical for test runs 74-96 and 74-97, the effective irradiance as a function of the distance from the beam centerline is

$$\mathcal{F}(r)=\mathcal{F}_0\exp(-r^2/w^2) \tag{18}$$

with $\mathcal{F}_0\simeq 1.8$ and $w\simeq 0.46$ cm in both instances. It is then a straightforward matter to obtain τ_V and $\Theta(1,\tau_V)$, at appropriately spaced radial distances, and to solve the differential equation (10) for $\tau_V\le\tau\le\tau_X$, keeping in mind that $\zeta_s(\tau_V)$ must always be set equal to zero; note that the position of the crater's edge r_c derives from

$$\tau_V(r_c)=\tau_X \tag{19}$$

and, thus, provides a ready check on the suitability of Eq. (18). The results of two such calculations ($t_X=1.13$ and 1.49 s) are displayed in Fig. 4 (dashed lines) and are seen to match the crater profiles rather poorly. Each data point corresponds to four measurements, as explained in Sec. II, the horizontal bar reflecting the observation that most of the craters were slightly oblong in the "north-south" direction, presumably because the laser beam impelled the ablator at an angle from the normal. At any rate, various attempts made to improve the fit, including insertion of the polynomial [Eq. (2a)] instead of the Gaussian [Eq. (2b)], were unsuccessful.

At this junction, three comments are believed to be relevant. 1) Presently available code-based modeling[6,16] exhibits similar deficiencies in the sense that penetrations at intermediate radial distances are too deep. 2) For 15-mm-diam targets, and no other adjustable parameter but the coupling coefficient, the HBI method delivers the same contours as elaborate finite-difference codes (see Ref. 5), thus demonstrating that the problem is of a generic nature. 3) The two broken profiles in Fig. 4 fit the data in the central region of the crater and at the edge. All of this suggests that the deficiency comes about because the models implicitly assume the effective irradiance remains constant during the entire burn, which cannot be correct in the later stages, when the crater begins to exhibit a significant slope. In other words, it appears indicated to rewrite Eq. (11) with $\mathcal{F}(r)\cos(\theta)$ replacing $\mathcal{F}(r)$ and θ measuring the angle between ablating surface and horizontal at station r. Unfortunately, this prescription injects additional complications in terms of computational procedures and appears to be difficult to mechanize. The best way to handle the situation consists in dividing the total exposure time into equal time intervals ($\tau_V,\tau_1,\tau_2,\ldots,\tau_X$) and to sequentially integrate ($\tau_i\le\tau\le\tau_{i+1}$) the differential

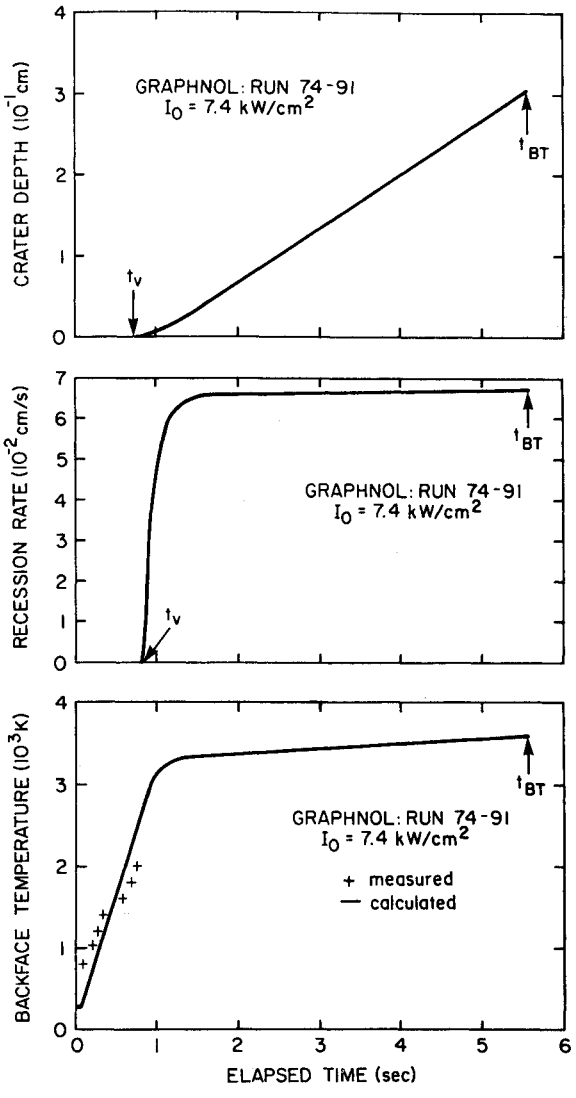

Fig. 6 Calculated, on-axis laser ablation history: test run 74-91.

equation

$$\frac{d}{d\tau}[\zeta_s(\tau)] = \frac{3}{\pi^2\eta}\left\{1-\Theta(1,\tau_V) - \frac{1-\Theta(1,\tau_V)+(e\eta/2)\zeta_s(\tau)-[e\mathcal{F}(r)/(2\pi^2)]\cos(\theta_i)(\tau-\tau_V)}{[1-\zeta_s(\tau)]^2}\right\} \tag{20}$$

where $\cos(\theta_i)$ is given by

$$\cos(\theta_i) = [1+|l\,d\zeta_s(\tau_i)/dr|_r^2]^{-1/2} \tag{21}$$

for all radial distances of interest, τ_V and $\theta(1,\tau_V)$ are as earlier, but initial values must be set equal to $\zeta_s(\tau_i)$. In practice, we found it quite convenient to approximate the ablation profile at time τ_i by means of a Chebyshev polynomial and to extract the derivative with the help of appropriate software. The results are displayed in Fig. 4 (solid curves) and are self-explanatory: There is a definite improvement in the agreement between theory and experiment, especially in the burnthrough case, which strongly supports the requirement of always incorporating the "cos(θ) correction" in calculations of this sort.

Similar work is presented in Fig. 5, which concerns the three test runs carried out at a peak intensity of about 7.5 kW/cm^2 (see Table 1). For convenience, it is assumed here that

$$\mathcal{F}(r) = 0.51\exp[-(r/0.462)^2] \tag{22}$$

is an acceptable expression for the effectively coupled beam intensity, and we then proceed in the same manner as previously, using Eqs. (20) and (21). The solid curves in Fig. 5 display the results and illustrate how the penetration progresses as the exposure increases to 5.84 s, in four equal time segments. For test run 74-91, which went slightly beyond burnthrough (5.84 vs 5.55 s), the fit is outstanding and reproduces the inverse conical shape of the crater; such agreement demonstrates our basic understanding of the interaction phenomenology, but should not be construed as a sensitive test of our ability to model ablation dynamics. The agreement also holds for shallow penetrations (see Fig. 5), keeping in mind that run 74-93 was set to last 2.2 s. There is, however, a problem with run 74-92 ($t_X = 4.4$ s), which is also apparent in code-based work performed at Physical Sciences Inc.[6] and may, therefore, be attributed to causes other than the methodology.

For the sake of completeness, we also present (see Fig. 6) the crater-depth, the recession-rate, and the backface-temperature history of a GraphNOL burnthrough at 7.4 kW/cm^2 in the standard geometry (15×3 mm). The nearly constant ablation rate over much of the exposure should not be perceived as indicative of a Phase II-type steady-state situation (semi-infinite slab!); the burn proceeds at a constant velocity because the backface has almost reached sublimation conditions by the time the front surface takes off. By means of a rapid-response imaging pyrometer, we were able to monitor the early backface surface-brightness evolution and to ascertain that, in the preablation phase, the temperature rise is indeed as anticipated.

V. Large Targets

The objective of test run 75-48 was to "quantify" radial conduction effects[7] by performing a burnthrough experiment on a 30-mm-diam specimen; such "large" targets do not verify the thermal equilibrium condition (λ is $< D/2$) and, therefore, may not obey the pattern described in Sec. IV. Judging from centerline effective irradiances as well as normalized exposure times, runs 75-48 and 74-96 are strictly identical and, therefore, should both obey the centerline ablation dynamics described in Fig. 3. The two ablation profiles, however, differ quite appreciably (see Fig. 7): The 30-mm target exhibits steeper crater walls, which suggests that an additional fraction of deposited laser energy was removed through enhanced lateral heat losses throughout the burn.

At this point, it should be of interest to reconsider the energy-balance relation that holds at the surface of an ablator in the absence of plume absorption:

$$I(r) = I_R(r) + I_A(r) + I_L(r) \tag{23a}$$

where I_R, I_A, and I_L refer to the beam-power densities dissipated in reflection, ablation, and losses, respectively. In terms of the target spectral emissivity α and the effective coupling coefficient α_{eff}, Eq. (23a) becomes

$$I(r) = (1-\alpha)I(r) + \alpha_{\text{eff}}I(r) + I_L(r) \tag{23b}$$

which demonstrates that, in principle, α_{eff} is a function of the radial distance r and can be expressed as in Eq. (1), i.e.,

$$\alpha_{\text{eff}}(r) = \alpha - I_L(r)/I(r) \tag{24}$$

keeping in mind that I_L is made up of contributions stemming from one-dimensional reradiation effects associated with axial transport and two-dimensional thermal effects caused by radial conduction. It is, of course, very com-

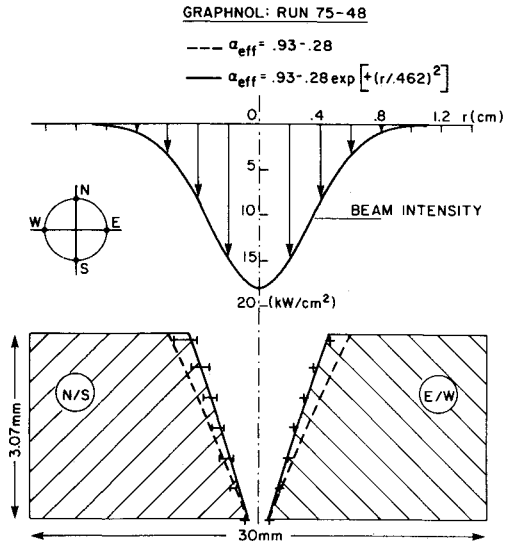

Fig. 7 Measured and calculated ablation profiles; the dashed lines reproduce the burnthrough crater of a 15-mm-diam specimen as in Fig. 4.

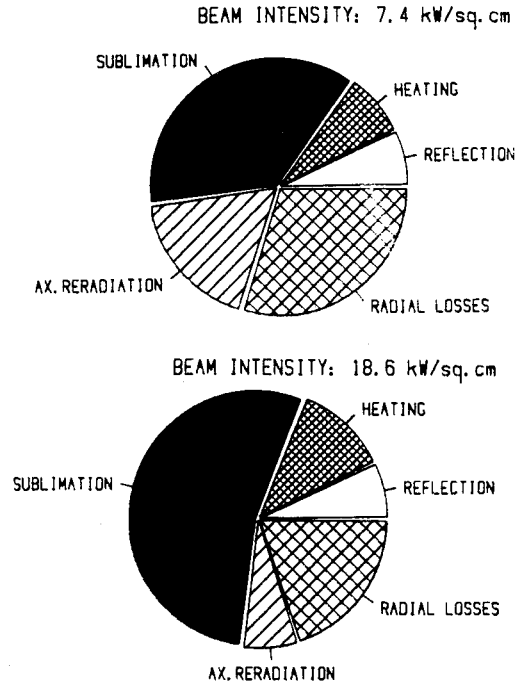

Fig. 8 Energy partitioning of two GraphNOL laser-irradiation experiments: $D = 15$ mm, $l = 3$ mm target.

plicated to properly describe heat losses occurring in the course of a nonstationary event such as ablation[17]; still, if one assumes that two-dimensional effects dominate, we have

$$I_L(r) \simeq -K(\partial T/\partial r)_{\text{crater}} \tag{25}$$

which relates the radial flow to the temperature gradient at the crater wall. In this light, it follows that a position-independent α_{eff}, which was seen in Sec. IV to be compatible with experimental observations (Figs. 4 and 5), immediately implies that the ratio $I_L(r)/I(r)$ is independent of r; this, in turn, implies that, in a thermal equilibrium situation ("small" target), we have $(\partial T/\partial r)_{\text{crater}} \propto I(r)$. For "large" targets, and since α_{eff} obviously decreases toward the edge of the crater (see Fig. 7), we may proceed heuristically and set $I_L(r)$ equal to $I_L(0)$. This amounts to postulating that $(\partial T/\partial r)_{\text{crater}}$ is approximately constant in a nonequilibrium situation and, by the same token, to assume that

$$\alpha_{\text{eff}}(r) = \alpha - I_L(0)/I(r) \tag{26}$$

for a "large" target such as the 30-mm-diam GraphNOL specimen used in conjunction with test run 75-48.

In this framework, the dimensionless irradiance $\mathfrak{F}$ becomes a function of the radial distance best expressed as follows:

$$\mathfrak{F}(r) = \mathfrak{F}_0 \exp(-r^2/w^2)\alpha_{\text{eff}}(r)/\alpha_{\text{eff}}(0) \tag{27a}$$

where $\mathfrak{F}_0$ is the centerline effective irradiance. Since the spectral emissivity α is approximately equal to 0.93,[14] and since Eq. (4) yields $\alpha_{\text{eff}} = 0.65$ on axis, we take it that, in the range $0 \le r \le 0.506$, an expression such as

$$\mathfrak{F}(r) = 2.78[0.93 \exp(-r^2/0.462^2) - 0.28] \tag{27b}$$

should be appropriate for test run 75-48. Proceeding now as previously, with the $\cos(\theta)$ correction properly carried out, the solution of Eq. (20) gives rise to the ablation profile displayed in Fig. 8 (solid lines); it is seen that the agreement with recorded crater-depth data is remarkable, particularly along the "east-west" direction, where the crater exhibits good symmetry.

It remains to be established that a position-dependent coupling coefficient as defined in Eq. (26) is indeed meaningful. For this purpose, we may consider the beam power falling on the crater, at burnthrough,

$$P_C = 2\pi \int_0^{r_c} I(r) r dr \tag{28}$$

and the power that is consumed in ablating the target,

$$P_A = 2\pi \int_0^{r_c} \alpha_{\text{eff}}(r) I(r) r dr \tag{29}$$

An average α_{eff} defined as follows:

$$\langle \alpha_{\text{eff}} \rangle = \int_0^{r_c} \alpha_{\text{eff}}(r) I(r) r dr \Big/ \int_0^{r_c} I(r) r dr \tag{30}$$

then measures the fraction of incident beam energy used up in penetrating the target, on assuming that the energy-partition process is essentially time independent. With an $\alpha_{\text{eff}}(r)$ as specified in the previous paragraph, and a crater radius as obtained by solving Eq. (19), we find that, for test run 75-48, the weighted average coupling coefficient $\langle \alpha_{\text{eff}} \rangle$ was close to 0.51. In terms of an effective heat of ablation based on mass loss (Q_m^*), that is, the laser energy required to remove a unit mass of material in a specific experimental configuration, it follows that

$$Q_m^* = H_A / \langle \alpha_{\text{eff}} \rangle \simeq 64 \text{ kJ/g} \tag{31a}$$

A direct evaluation of Q_m^* from the total radiation energy that fell on the crater and the mass of material that was removed by sublimation, or

$$Q_m^* = \left[2\pi \int_0^{a_1} I(r) r dr\right] t_X \Big/ \left[\left(\frac{1}{3}\right) \pi h (a_1^2 + a_1 a_2 + a_2^2)\right] \rho \tag{31b}$$

if the crater is modeled as the frustrum of a circular cone, yields $Q_m^* \simeq 69$ kJ/g; considering the many uncertainties involved in obtaining these two Q_m^*'s, particularly with regard to α, I_0, and H_A, the "correlation" appears to be satisfac-

tory, thus providing further justification for injecting an $\alpha_{\text{eff}}(r)$ as specified earlier [Eq. (26)].

VI. Discussion and Conclusion

The laser-effects community makes use of the concept of an effective heat of ablation, Q^*, to assess experimental data and to characterize the ability of target materials to "defeat" incident laser radiation. The definition of a meaningful Q^*, for a specific interaction environment, is predicated upon a steady-state situation at the ablation front and relates immediately to our effective coupling coefficient ($Q^* = H_A/\alpha_{\text{eff}}$) if α_{eff} accepts an objection-free interpretation as in the case of flood-loaded targets. For run 74-96, this would indicate that "$Q^* = 49$ kJ/g" is indeed a valid statement; along the same line, we may add that

$$Q^*_\infty \equiv \lim_{I_L/I \to 0} [Q^*(I)] = H_A/\alpha \tag{32}$$

amounts to 35 ± 3 kJ/g for GraphNOL (see Table 2), which is in agreement with a "theoretical Q^*" for polycrystalline graphite, as reported in Ref. 18.

In the context of energy-partition considerations, we emphasize that the fractions of incident laser-fluence dissipated in various processes can be ascertained easily from the sequence

$$\begin{aligned} &\text{Reflection:} && I_R/I = 1-\alpha \\ &\text{Ablation:} && I_A/I = \langle \alpha_{\text{eff}} \rangle \\ &\text{Losses:} && I_L/I = \alpha - \langle \alpha_{\text{eff}} \rangle \end{aligned}$$

in conjunction with Table 3. Furthermore, if we recall that 1) axial reradiation losses can be approximated by means of the relation

$$\mathcal{P} = [\epsilon_F + \epsilon_B (\bar{T}_B/T_V)^4] \sigma_{\text{SB}} T_V^4 \tag{33}$$

and 2) sublimation takes up $\eta/(1+\eta)$ percent of the ablation enthalpy, it becomes a straightforward matter to subdivide the "ablation" and "loss" shares. Figure 8 demonstrates how this works and illustrates the impact of beam intensity on energy partitioning in laser-irradiated GraphNOL: The fraction of incident fluence dissipated in sublimating our "standard" targets amounts to 37% at a peak intensity of 7.4 kW/cm^2 but rises to 54% at 18.6 kW/cm^2, in accord with the intuitive notion that, relatively speaking, thermal losses will be much enhanced at lower irradiance levels.

In summary, this work provides conclusive evidence that, with no other adjustable parameter but the coupling coefficient, analytic HBI-based procedures can deliver solutions of laser-ablation problems that are equivalent to solutions generated by means of finite-difference-based codes.[6,16] Although laser heating and laser ablation are both far more complex than simple models would lead us to believe, the agreement with experimental results appears to be satisfactory, which is quite remarkable considering the rather crude approximations associated with HBI methodologies. The present analysis pivots around three dimensionless parameters:

$$\tau_X = \pi^2 \kappa t_X / l^2, \quad \mathcal{F} = \alpha_{\text{eff}} Il/(\bar{K} T_V'), \quad \eta = H_V/(\bar{C}_p T_V') \tag{34}$$

which were found to be instrumental in identifying some key features of the interaction process.

1) In the present experiments, backface heating occurs prior to the onset of front-surface recession, and we have shown how the integral method can be applied to devise an elegant description of crater formation and target burnthrough under such conditions.

2) A satisfactory match between calculated and recorded ablation profiles requires some care in the sense that the procedure outlined in Ref. 5 must be amended to reflect the progressive "degradation" in irradiance as the beam penetrates deeper into the target.

3) Finally, we have shown that problems regarding the crater formation in "large" targets, that is, targets for which the lateral diffusion time becomes comparable to the total exposure time, can be resolved by means of a straightforward alteration of the lateral heat-loss dependence on radial distance.

Acknowledgments

This work was sponsored by the Defense Advanced Research Projects Agency under Subcontract BDM-S308-OL7200 to The BDM Corporation (Prime Contract MDA903-82-C-0359) and Subcontract PSI-P.O.-SC8288 to Physical Sciences Inc. (Prime Contract MDA903-85-C-0123).

References

[1]Ready, J. F., *Effects of High-Power Laser Radiation,* Academic Press, New York, 1971, Chap. 3.

[2]Rykalin, N. N. and Uglov, A. A., "Thermophysical Processes in the Interaction of Laser Radiation with Absorbing Media," *Bulletin of the Academy of Sciences of the USSR, Physics Series,* Vol. 46, No. 6, 1982, pp. 8–14.

[3]Goodman, T. R., "Application of Integral Methods to Transient Nonlinear Heat Transfer," *Advances in Heat Transfer: Vol. 1,* Academic Press, New York, 1964, pp. 51–122.

[4]Harrach, R. J., "Analytical Solutions for Laser Heating and Burnthrough of Opaque Solid Slabs," *Journal of Applied Physics,* Vol. 48, No. 6, June 1977, pp. 2370–2383.

[5]Klein, C. A., "Analytical Modeling of Laser-Ablated Sublimators: The Heat-Balance Integral Method," AIAA Paper 84-1782; also *AIAA Journal,* Vol. 25, Jan. 1987, pp. 48–49.

[6]Popper, L., Frish, M., Modak, A., and Pirri, A., "Analysis of Ablation Data," presented at LCMMD Workshop, La Jolla, CA, Physical Sciences Inc., Andover, MA, July 1983.

[7]Stickley, M., et al., "Laser Counter-Measure Materials Development Program: First Technical Report," The BDM Corp., McLean, VA, Rept. BDM/W-83-414-TR, June 1983.

[8]Cunningham, J. E., "Recent Developments in Graphite," ORNL, Oak Ridge, TN, Rept. CONF-830336-1, March 1983.

[9]Klein, C. A. and Berry, M. J., "Small-Scale Laser Effects Experiments on Graphite: Coupling Coefficient, Lateral Loss, and Effective Heat of Ablation," *Journal of Applied Physics,* March 1987.

[10]Marquardt, D. W., "An Algorithm for Least-Squares Estimation of Nonlinear Parameters," *Journal of the Society of Industrial and Applied Mathematics,* Vol. 11, 1963, pp. 431–441.

[11]Crane, K. C. and Brown, J. R., "Laser-Induced Ablation of Fiber/Epoxy Composites," *Journal of Physics D: Applied Physics,* Vol. 19, 1981, pp. 2341–2349.

[12]Baker, R. L. and Covington, M. A., "The High-Temperature Thermochemical Properties of Carbon," Space Division, AFSC, Los Angeles, CA, Rept. SD-TR-82-19, March 1982.

[13]Johnson, B. B. and Starrett, H. S., "Preliminary Design Data Package for GraphNOL N_3M," Southern Research Institute, Birmingham, AL, Rept. SoRI-MER-82-20, Nov. 1982.

[14]Frish, M. B., "Measurement of High-Temperature Thermophysical Properties with Electron-Beam Heating," AIAA Paper 84-1784, 1984.

[15]Carslaw, H. S. and Jaeger, J. C., *Conduction of Heat in Solids,* Oxford University Press, London, 1959, Chap. 3.

[16]Grant, S. D., "Status of the ASTHMA/BMD Code," presented at LCMMD Workshop, La Jolla, CA, The BDM Corp., McLean, VA, July 1983.

[17]Sparks, M., "Analysis of Preliminary Data from Raytheon/UTRC Tests," Scientific Research Center, Los Angeles, CA, Working Note WN:bdm-8316, April 1983.

[18]Lundell, J. H. and Dickey, R. R., "Response of Heat-Shield Materials to Intense Laser Radiation," *Progress in Astronautics and Aeronautics:* Vol. 64, AIAA, New York, 1978, pp. 193–209.